Self-assembly and Temperature-driven Chirality Inversion of Cholesteryl-based Block Copolymers

Velmurugan Krishnasamy[a], Wentao Qu[a], Changlong Chen[a], Haohui Huo[a], Karthick Ramanagul[b], Velraj Gothandapani[b], Georg H. Mehl[a,c], Qilu Zhang[a*], Feng Liu[a*]*

[a] State Key Laboratory for Mechanical Behaviour of Materials, Shaanxi International Research Center for Soft Matter, Xi'an Jiaotong University, Xi'an 710049 (P. R. China)

[b] Department of Physics, Anna University, Chennai, India

[c] Department of Chemistry, University of Hull, Hull HU6 7RX, UK.

KEYWORDS: block copolymer, cholesterol, liquid crystals, self-assembly, chirality inversion

ABSTRACT

Block copolymers (BCPs) comprising of a poly(methyl methacrylate) (PMMA) block and a poly(cholesteryloxyhexyl methacrylate block (PChMA) were synthesized *via* reversible addition-fragmentation chain transfer (RAFT) polymerization. The self-assembly of the liquid crystalline block copolymers was characterized by differential scanning calorimetry (DSC),

polarized optical microscopy (POM) and synchrotron-based small-angle X-ray scattering (SAXS). The results indicate the formation of both tilted and non-tilted chiral smectic (SmC* and SmA*) phases. A phase transition from SmA* to SmC* phase on cooling was observed for BCPs, but not for PChMA homopolymers. The layer spacing (5.00 ± 0.18 nm) between those can be controlled to maintain the number of ChMA units whilst varying the lengths of the PMMA block, introducing thus systematically the SmC* phase. Furthermore, BCPs with short PMMA block showed inversion of chirality at specific temperatures; while for PChMA attached with long PMMA block no chirality inversion was observed. This mode of chirality switching, investigated by CD, NMR, and theoretical studies, is associated with the methyl substituents in the backbone affecting the packing of the polymers. The basic rules, described here, have the potential to be implemented for the design of a wide range of functional materials where helix-helix conversion is of use.

INTRODUCTION

The research on polymers with liquid crystalline (LC) pendants has emerged as one of the major topics in materials science.[1-8] The combination of BCP topology and LCs is expected to allow for the design of advanced features in functional materials, allowing thus miniaturization of domain spacing in nanoscopic materials, high processability and the designing of novel morphologies.[9-12] In addition, the introduction of chiral functionality to LCPs has become one of the most important topics in LC research as it may permit the introduction of chiral nanostructures due to chiral amplification. The combination of LC polymers with chiral

mesogens may result in chiral soft materials with superior properties and applications as, e.g. electronic and photonic materials.

LC block copolymers (BCPs) are the combination of LC mesogens with non-liquid crystalline and incompatible blocks. One of the most reported LC-BCPs is rod-coil BCPs[13,14] and this architecture permits the systematic shrinking in volumes. More specifically, rod-coil BCPs containing LC groups can combine the rigidity of the mesogenic part with the higher flexibility of the soft block and improve the chain stretching. For well-defined systems a corona-like shell around the LC block can generate nanophase separation of LC blocks resulting in complex phase behaviour and extremely small domain volumes. Interestingly LC-BCPs can act as a unique candidate for the analysis of the impact of an additional level functionality in the rigid core on the organization of well-defined macromolecular assemblies. In addition, internal LC ordering can be tuned from a less-ordered nematic or cholesteric phase to high-ordered smectic phase by changing the synthetic strategy of LC blocks or other coinciding parameters.[15,16]

Chirality switching has been observed in the case of optically active small molecules and polymers by a range of external stimuli, such as temperature, photoisomerization, pH, the addition of chiral dopants and solvent polarity.[17-20] Temperature as a stimulus for chirality switching is very attractive as the temperature can typically be measured and controlled with high precision and the response is usually fast. Moreover, it removes the requirement for increasing the complexity of the investigated system by the incorporation of trigger or switching moieties; hence this approach has been termed additive free.[21,22] Fujiki et al[23,24] reported an optically active helical polysilylene comprising a rod-like main chain, undergoing a thermo-driven chirality inversion in dilute isooctane solution. In addition, Tang et al[25] reported

helical-switching polymers such as poly(*n*-hexyl isocyanate) used as chiral dopants in lyotropic liquid crystals and observed the helical-twist phenomenon as a function of temperature.

Here we demonstrate another mechanism for controlled chirality switching without any additional chiral dopants exists, which to the best of our knowledge, has not been reported yet. It is based on the temperature controlled packing frustration of suitably selected block copolymers consisting of side-chain liquid crystal and aliphatic blocks of carefully defined dimensions. Our results are shown for a specific set of materials, however, as the driving for the chirality inversions are related to the rearrangement of what are essentially hydrocarbon blocks; we anticipate that the approach can be extended to other materials. To show the general versatility of the concept we utilized an optimized system, consisting of the ubiquitously employed cholesteryl group as a chiral and mesogenic unit separated from a methacrylate main chain by a hexyl spacer. For the other block, a simple coil poly(methylmethacrylate) chain was selected. We note here that the investigated system does not contain aromatic groups and is hence transparent at wavelengths above ~ 320 nm allowing thus for the future inclusion of further functionality.

Specifically, we report here the synthesis of a series of LC-BCPs by reversible addition-fragmentation chain transfer (RAFT) polymerization; the full chemical characterization of the polymer properties, including the tacticity of the main chain by detailed NMR studies, as well as the characterization of the LC properties by temperature dependent polarizing optical microscopy (POM), differential scanning calorimetry (DSC) and synchrotron-based small-angle X-ray scattering (SAXS) studies. The chirality and temperature dependent chirality inversion were measured by circular dichroism (CD) measurements of thin films whose thicknesses were determined by profilometry. The analysis of the results was underpinned by detailed simulation

studies relating spectroscopic data to molecular conformation; the molecular conformations and their assemblies are responsible for the changes of chirality inversion. The polymerization reaction was carried out by reversible addition-fragmentation chain transfer (RAFT) polymerization of 4-cyanopentanoic acid dithiobenzoate (CPADB), enantiomerically pure cholesteryl methacrylate (ChMA) as well as methylmethacrylate (MMA) as monomers using azobisisobutyronitrile (AIBN) as an initiator and toluene as a solvent. The PChMA macroinitiators bearing cholesterol moieties were first obtained from the RAFT polymerization of enantiomerically pure ChMA monomer using the RAFT agent (CPADB) and then utilized in the preparation of LC-BCPs (PChMA -*b*-PMMA) with various DPs (*N*).

EXPERIMENTAL SECTION

Synthesis of cholesteryloxyhexyl methacrylate (ChMA)

Cholesteryloxyhexanol (Ch-OH) (0.5 g, 1.0 mmol) in dichloromethane (20 ml), methacryloyl chloride (0.15 ml, 1.5 mmol) and triethyl amine (0.42 ml, 3.1 mmol) were stirred at room temperature for 6 h. Upon completion, the reaction mixture was extracted with dichloromethane, washed with brine and concentrated by rota-evaporation. The crude mixture was then purified by silica gel column chromatography using petroleum ether:ethylacetate (9:1) solvent mixture, obtained as cholesteryloxyhexyl methacrylate (ChMA) with high enantiomeric purity (99 %).[26] Yield: 0.4 g (71 %). ^{1}H NMR (600 MHz, $CDCl_3$): δ 6.09 (s, 1H), 5.54 (s, 1H), 5.35 (m, 1H), 4.13-4.15 (t, 2H), 3.42-3.48 (m, 2H), 3.09–3.15 (m, 1H), 2.34–2.39 (m, 1H), 2.16–2.20 (m, 1H), 1.94–2.03 (m, 5H), 1.25–1.89 (m, 23H), 0.86-1.17 (m, 21H), 0.68 (s, 3H) ppm.

Synthesis of macro-CTA ($PChMA_{12}$)

All of the homo (PChMA) and block copolymers (PChMA-*b*-PMMA) were obtained by RAFT polymerization and the detailed procedures are depicted in the following examples.

A typical procedure for the synthesis of PChMA is as following: enantiomerically pure monomer ChMA (1.98 g, 3.7 mmol), 4-cyanopentanoic acid dithiobenzoate (CPADB) (69 mg, 0.2 mmol), AIBN (14 mg, 72.7 μmol) and toluene (3 ml) were added to a Schlenk tube equipped with a stirring bar. The reaction mixture was degassed by three freeze-pump-thaw cycles, and sealed under nitrogen. This reaction tube was placed in an oil bath preheated at 80 °C for 2 h, and the reaction mixture was quenched by dipping the reaction tube in ice. The mixture was precipitated by methanol and dried under reduced pressure. The polymer product was a pale pink colored solid. The degree of polymerization (DP) of the polymers was calculated by DP=[M]/[CTA]**c*, where [M] and [CTA] are the concentration of monomer and CTA, respectively, and *c* represents the conversion of monomer quantified by ^{1}H NMR in $CDCl_3$. The number average molecular weight (M_n) and the dispersity ($Đ$) were analyzed by size exclusion chromatography (SEC) using polymethylmethacrylate (PMMA) as calibration standard.

A typical procedure for the synthesis of PChMA-*b*-PMMA is as following: $PChMA_{12}$ (0.50 g, 71.9 μmol), methyl methacrylate (0.28 g, 2.8 mmol), AIBN (2.20 mg, 14.1 μmol) and toluene (0.5 ml) were placed in a Schlenk tube. The mixture was degassed by three freeze-pump-thaw cycles and sealed under nitrogen. The reaction tube was placed in an oil bath at 70 °C for 6 h and the reaction was quenched by dipping the tube in ice. The mixture was precipitated in hexane and dried under reduced pressure. The polymer product was a colorless solid. We note that different temperatures were applied for the polymerization of the two monomers, i.e. ChMA and MMA are polymerized at respectively, 80 °C and 70 °C. Such

differences in the reaction temperatures are needed as suggested by test reactions. For ChMA homopolymers, we observed that when setting the reaction temperature at 70 °C in initial trials, the polymerization rates were very low, yielding broad molecular weight distributions of the resulted polymers. Such slow reactions may be due to the steric hindrance of the bulky cholesteric units. Hence, a high temperature was applied for ChMA polymerization to allow faster reactions. In contrast, MMA polymerizations were performed at 70 °C, which is a typical temperature for methacrylate polymerization mediated by the RAFT mechanism with AIBN as initiator. Indeed polymerizations at 80 °C were also explored initially and we detected that the reactions rates were to too fast resulting in poor control of the polymer structure. Hence, the reaction temperature for the preparation of homo and block copolymers were set at 80 °C and 70 °C, respectively.

RESULTS AND DISCUSSION

Synthesis of cholesterol based LC polymers

A series of cholesterol derived LC polymers were prepared by polymerization of tailor-made enantiomerically pure cholesterol monomer, *via* reversible addition-fragmentation chain transfer (RAFT) polymerization,[27,28] which allows the preparation of block copolymers with well-defined structures (Scheme 1). Initially, LC monomer, enantiomerically pure cholesteryloxyhexyl methacrylate (ChMA) was prepared by the esterification of methacryloyl chloride with cholesteryloxyhexanol. The success synthesis and purification of the target monomer were confirmed by ^{1}H NMR and HPLC (Figure S1). Then the cholesterol-based homopolymers (PChMA) with DP's of 12, 24 and 40 (determined by ^{1}H NMR) were prepared by RAFT

polymerization mediated by CPADB as chain transfer agent (CTA). The obtained PChMA homopolymers were further utilized as a macromolecular CTA (macro-CTA) to mediate the polymerization of MMA, which lead to cholesterol-based block copolymers with defined DPs, PChMA-*b*-PMMA. ^{1}H NMR spectra of the polymerization solutions were used to determine the conversions of the monomers, which were further used to calculate the DP's and absolute molar mass ($M_{n,\mathrm{NMR}}$) of the copolymers. The resulting block copolymers were characterized by ^{1}H NMR, size-exclusion chromatography (SEC) (Figures S2 and S3) and the results are summarized in Table 1. Characteristic resonance signals for both cholesterol groups from ChMA and methoxy (–OCH_3) groups from MMA are observed by ^{1}H NMR, in combination with the shift of SEC traces the data indicate the success of extending of PMMA on PChMA macro-CTAs. Number average molecular weight ($M_{n,\ \mathrm{SEC}}$) and its dispersity ($Đ$) of the polymer were calculated with PMMA as calibration and are shown in Table 1. Higher values of M_n from SEC were obtained than those calculated from NMR data. This can be ascribed to the relatively large coil size of PChMA-*b*-PMMA in THF when compared to the PMMA calibrator with the same molecular weight.[29] In addition, the $Đ$ values of the copolymers were also obtained, with most of the values lower than 1.35 indicating an acceptably good control of the polymerization *via* RAFT mechanism. We note that the slightly higher $Đ$ values than observed for typical RAFT polymers are however reasonable for the polymerization of bulky monomers, such as ChMA used for LC-BCP and in line with results obtained for other liquid crystal side-chains.[49] We attribute this to the steric hindrance of monomer units at the ω-end of the "living" polymer chains which may hinder the chain transfer efficiency of CTA. Such hindrance may occur in the RAFT polymerization of both ChMA and MMA at early stage.

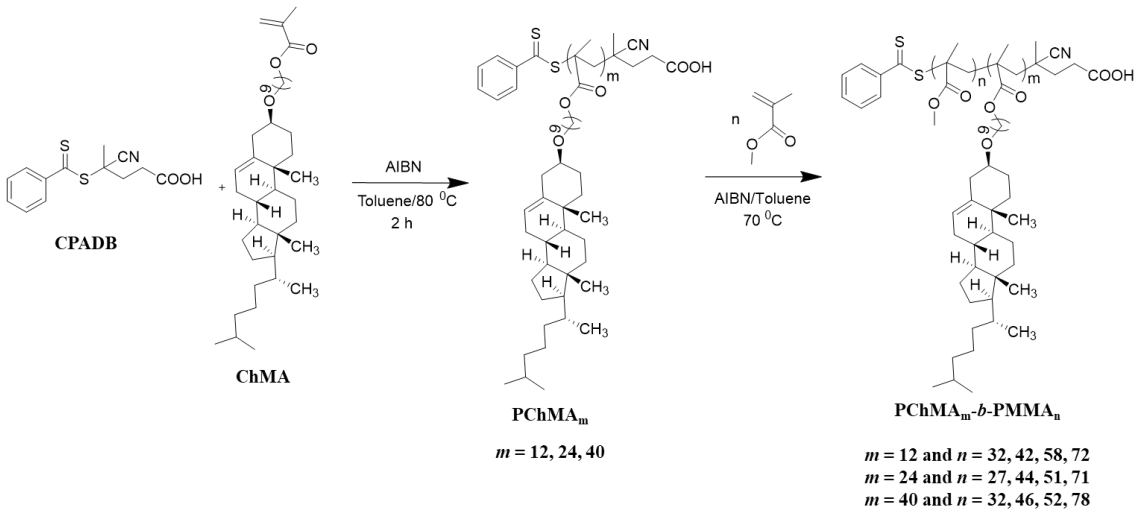

Scheme 1. Synthesis of cholesterol-based homo PChMA and PChMA-*b*-PMMA block copolymers by RAFT polymerization.

Table 1. Summary of M_n (SEC & NMR) and $Đ$ of LC-homo and block copolymers synthesized *via* RAFT polymerization.

Polymers	$M_{n,\,SEC}$ [a] kDa	$M_{n,\,NMR}$ [b] kDa	$Đ$ [a]
PChMA$_{12}$	17.2	6.9	1.14
PChMA$_{12}$-*b*-PMMA$_{32}$	20.4	10.1	1.17
PChMA$_{12}$-*b*-PMMA$_{42}$	22.3	11.1	1.24
PChMA$_{12}$-*b*-PMMA$_{58}$	21.9	12.8	1.33
PChMA$_{12}$-*b*-PMMA$_{72}$	21.3	14.2	1.38
PChMA$_{24}$	26.2	13.6	1.17
PChMA$_{24}$-*b*-PMMA$_{27}$	26.4	16.3	1.21
PChMA$_{24}$-*b*-PMMA$_{44}$	26.9	18.0	1.21
PChMA$_{24}$-*b*-PMMA$_{51}$	24.4	18.7	1.47
PChMA$_{24}$-*b*-PMMA$_{71}$	25.4	20.8	1.30

$PChMA_{40}$	33.4	22.5	1.27
$PChMA_{40}$-*b*-$PMMA_{32}$	33.9	25.7	1.27
$PChMA_{40}$-*b*-$PMMA_{46}$	39.8	27.1	1.39
$PChMA_{40}$-*b*-$PMMA_{52}$	33.4	27.7	1.30
$PChMA_{40}$-*b*-$PMMA_{78}$	38.1	30.4	1.22

[a]Number average molecular weight (M_n, SEC) and polydispersity ($Đ$) were calculated using SEC calibrated by poly(methylmethacrylate) (PMMA) standards. [b] Composition of the homo and block copolymers and M_n, NMR was determined by ^{1}H NMR spectra in $CDCl_3$.

Microstructure analysis and steric effects of the LC-BCPs were further evidenced by 1D and 2D NMR analysis. Carbonyl carbon resonance peak assignments of PChMA and PChMA-*b*-PMMA were clearly identified by NMR analysis (Figures 1 and S4-S6). $PChMA_{24}$ contains the three peaks of resonances at 176.02-176.18, 176.70 and 177.21 ppm assigned to mmrr+rmrr, rrrr and mrrr/rrrm pentads were similar to that stated by Brar et al[30] which indicates that most of the LC blocks are predominantly in the syndiotactic in their microstructure. In the case of LC-BCPs, such as $PChMA_{24}$-*b*-$PMMA_{27}$ the six peaks of resonances occurred at 175.98, 176.66-176.90, 177.04, 177.41, 177.71 and 178.01 ppm assigned to mmmm, mmrr+rmrr, mmrm+rmrm, rrrr, mrrr/rrrm and mrrm pentads.[31,32] Upon increasing the DP's of PMMA blocks in the $PChMA_{24}$-*b*-$PMMA_n$, all of the pentad peaks are shifted to the downfield region and their peak intensity is increased except in the case of rrrr pentad peak intensity, which is significantly decreased. Similar trends were observed in the case of $PChMA_{40}$ and their corresponding $PChMA_{40}$-*b*-$PMMA_n$ (Figure S7). The reason for the downshift of the peaks is at present not yet unambiguous. One possible, in our view likely explanation is that the C=O bond from the PMMA blocks can influences the electronic environment of the ChMA units, and hence results

in the shift of resonance peaks of carbonyl carbon of ChMA units. Based on these results, we deduced that PChMA blocks exist predominantly as syndiotactic species, which may be ascribed to the strong steric hindrance between the bulky LC mesogens. With the addition of an PMMA block, which is relatively soft and heterotactic, the overall syndiotactic species decreases with the increasing of the DP of MMA, as shown in Table S1). In addition to that, in the case of $PChMA_{40}$-*b*-$PMMA_{32}$, there are no intramolecular cross-peaks observed between the methoxy ($-OCH_3$) protons of PMMA and alkyl protons of the PChMA blocks in the NOESY analysis (Figure S8), which reveals that LC-BCPs with the low DP's of PMMA are typically present in anti-conformation. On the basis of above results, we concluded that PChMA blocks are predominantly present in syndiotactic forms.

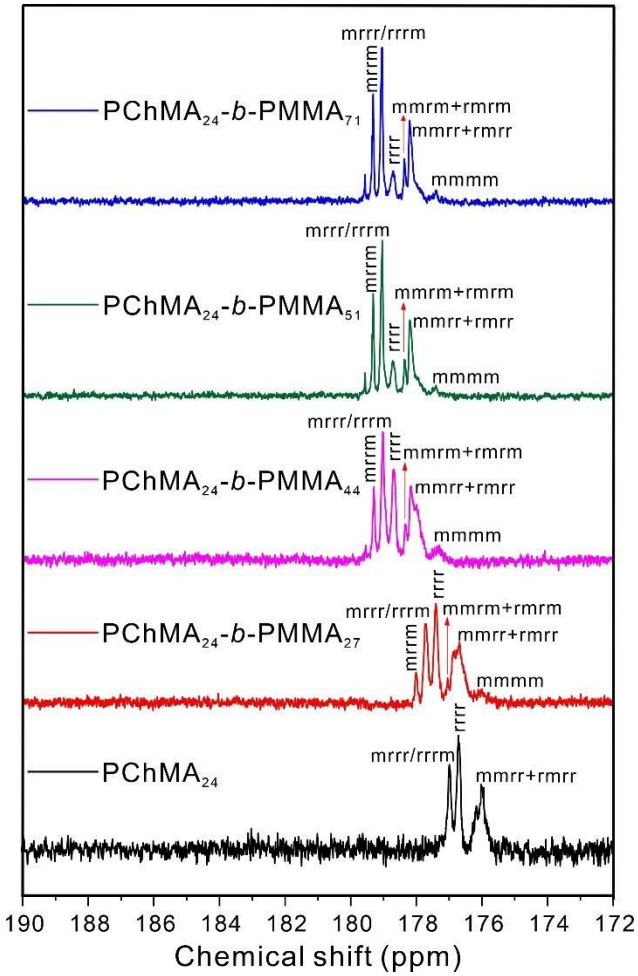

Figure 1. ^{13}C NMR spectrum of carbonyl carbon of $PChMA_{24}$ and $PChMA_{24}$-*b*-$PMMA_n$

Liquid crystalline performance of the cholesterol derived homo and BCPs

The LC properties of all the synthesized cholesterol-based homo- (macro-CTA) and block copolymers were fully evaluated by differential scanning calorimetry (DSC) and polarizing optical microscopy (POM) (For experimental details, see SI). All compounds form thermostable (enantiotropic) liquid crystalline phases from room temperature to the clearing points (Figure S9). The clearing-point enthalpies for the homo and BCPs emerge are somewhat broad due to a biphasic region which is a result of the dispersity (*Đ*) of the polymers and the presence of a non

LC isotropic block.[19] The phase transition temperatures and their corresponding enthalpies of all the homo- and block copolymers are summarized in Table 1. A clear shift of the phase transition temperatures of both homo and block copolymers to higher temperatures with increasing size of the polymers was found indicating a remarkable influence of the PMMA block on the phase behaviour of the polymers; in other words, the increase of the size of the non LC block enhances the stability of the LC phase.[33,34]

Table 2. Phase transitions behaviour of the cholesterol-based polymers

Polymers	Phase transitions/ °C (enthalpy changes/J g^{-1})[a] Heating (*H*)/Cooling (*C*)	[c]SmA*-helix inversion
$PChMA_{12}$	*H*: SmA* 108 (2.14) I *C*: I 99 (2.20) SmA*	-
$PChMA_{12}$-*b*-$PMMA_{32}$	*H*: SmC*[b] 50 (-) SmA* 118 (3.04) I *C*: I 109 (3.37) SmA* 45 (-) SmC*[b]	-
$PChMA_{12}$-*b*-$PMMA_{42}$	*H*: SmC*[b] 60 (-) SmA* 114 (2.86) I *C*: I 111 (2.56) SmA* 55 (-) SmC*[b]	-
$PChMA_{12}$-*b*-$PMMA_{58}$	*H*: SmC*[b] 60 (-) SmA* 120 (2.13) I *C*: I 111 (1.83) SmA* 50 (-) SmC*[b]	-
$PChMA_{12}$-*b*-$PMMA_{72}$	*H*: SmC*[b] 60 (-) SmA* 126 (3.56) I *C*: I 121 (2.69) SmA* 56 (-) SmC*[b]	-
$PChMA_{24}$	*H*: SmA* 98 (2.40) I *C*: I 88 (2.15) SmA*	
$PChMA_{24}$-*b*-$PMMA_{27}$	*H*: SmA* 131 (4.22) I *C*: I 119 (3.53) SmA*	Helix-inversion
$PChMA_{24}$-*b*-$PMMA_{44}$	*H*: SmC*[b] 55 (-) SmA* 132 (3.53) I	-

	C: I 118 (3.54) SmA* 50 (-) SmC*[b]	
PChMA$_{24}$-*b*-PMMA$_{51}$	*H*: SmC*[b] 60 (-) SmA* 120 (3.93) I	-
	C: I 109 (2.65) SmA* 55 (-) SmC*[b]	
PChMA$_{24}$-*b*-PMMA$_{71}$	*H*: SmC*[b] 60 (-) SmA* 117 (3.59) I	-
	C: I 106 (2.37) SmA* 52 (-) SmC*[b]	
PChMA$_{40}$	*H*: SmA* 121 (3.51) I	-
	C: I 112 (4.06) SmA*	
PChMA$_{40}$-*b*-PMMA$_{32}$	*H*: SmA* 134 (4.14) I	Helix-inversion
	C: I 122 (3.64) SmA*	
PChMA$_{40}$-*b*-PMMA$_{46}$	*H*: SmA* 100 (2.36) I	Helix-inversion
	C: I 87 (2.48) SmA*	
PChMA$_{40}$-*b*-PMMA$_{52}$	*H*: SmC*[b] 55 (-) SmA* 128 (3.58) I	-
	C: I 118 (3.62) SmA* 50 (-) SmC*[b]	
PChMA$_{40}$-*b*-PMMA$_{78}$	*H*: SmC*[b] 56 (-) SmA* 136 (3.46) I	-
	C: I 124 (3.95) SmA* 50 (-) SmC*[b]	

[a]Peak temperatures (°C) and enthalpies (J g^{-1}) were determined by a scanning rate of 10 K/min. SmC*, Chiral Smectic C; SmA*, Chiral Smectic A; I, Isotropic phase. [b]The SmC* phase was observed due to the formation of optical textures. [c]SmA-helix inversion was identified by CD analysis. (* indicates the presence of chiral mesogens in LC-BCPs)

All the compounds show birefringence under crossed polarizers. Upon cooling from the isotropic state, all homopolymers and short-chain BCPs (PChMA$_{24}$-$_{b}$-PMMA$_{27}$, PChMA$_{40}$-*b*-PMMA$_{32}$ and PChMA$_{40}$-*b*-PMMA$_{46}$) showed the formations of *batonnêt* textures upon annealing at various temperatures (Figure 2), which indicates the emergence of a layered phase with the molecules on average positioned perpendicular to the layer normal (SmA), and, as

the molecules are chiral, identified as a SmA* phase. On cooling most of the LC-BCPs exhibit *schlieren* textures with four brush (s = ±1) defects forming at the SmA* to SmC* transition (Figures 2f and S10-S12). This indicates that a phase transition from SmA phase to a phase where the mesogens are tilted with respect to the layer normal has taken place; the formation of only four brush defects excludes a re-entrant nematic phase or the simple onset of interdigitation. The simplest and most natural assignment is that of the formation of a SmC* phase, as the molecules are chiral; eschewing more complex phase structures.. [Marcelis, A.; Koudijs, A.; Sudhölter, E.; Mol. Cryst. Liq. Cryst. 2004, *411*, 193-200; Majumdar; K.C.; Mondal, S.; Sinha R. K.; *New. J. Chem*. 2010; *34*, 1255-1300] At temperatures below the transition, incident plane-polarized light is rotated by the textures indicating that these phases are helical[35] (Figures S13 and S14), supporting the assignment as SmC*.

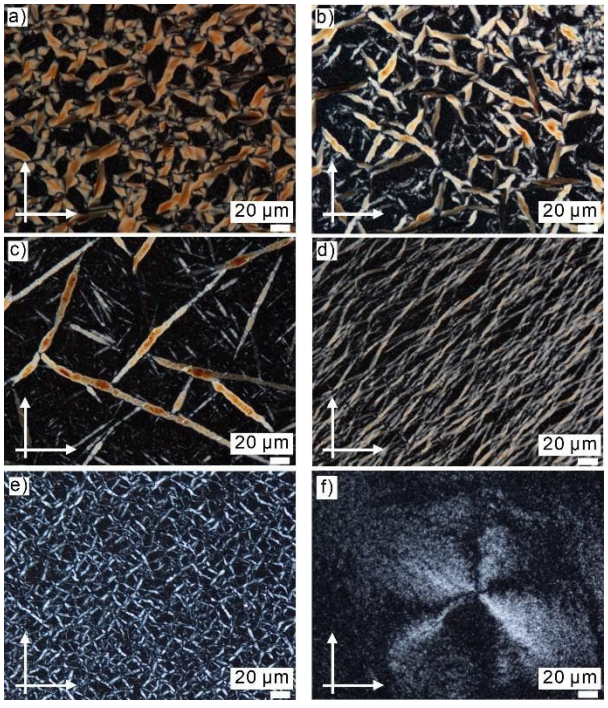

Figure 2. POM images of LC-homo and BCPs under crossed polarizers *batonnet* textures of a) $PChMA_{24}$ (annealed at 100 °C); b) $PChMA_{40}$ (annealed at 120 °C); c) $PChMA_{24}$-*b*-$PMMA_{27}$ (annealed at 120 °C); d) $PChMA_{40}$-*b*-$PMMA_{32}$ (annealed at 130 °C); e) $PChMA_{40}$-*b*-$PMMA_{46}$ (annealed at 100 °C); f) *Schlieren* textures of $PChMA_{40}$-*b*-$PMMA_{78}$ with four brush defects at 50 °C (Scale = 20 μm).

In order to investigate the phase sequence of LC phase structures of these LC homo and block copolymers, temperature-dependent synchrotron-based small/wide-angle X-ray scattering experiments were performed for all the compounds. The sharp peaks with a ratio of 1:2:3 in the small-angle X-ray region indicate that all of the polymers form layered mesomorphic superstructures, i.e., smectic phases; unfortunately GISAXS experiments on thin films did not offer well-oriented diffraction patterns as observed under different experimental conditions for elastomers.

Wen, Z.B.; Liu, D.; Li, X.Y.; Zhu; C.H.; Shao, R. F. Visvanath, R.; Clark, N. A.; Yang, K. K.; Wang, Y. Z.; *ACS Appl. Mater. Interfaces* 2017, 9, 24947−24954;

Li, Y.; Zhang, Y.; Goswami, M.; Vincent, D.; Wang, L.; Liu, T.; Li, K.; Keum, J.K.; Gao, Z.; Oczan, S.; Gluesenkamp, K.R.; Rios, O.; Kessler, M. R. ; *Soft Matter,* 2020, *16,* 1760-1770

We note too that the data does not show the signals typically associated with the formation of a superstructure based on microsegregated blocks. The diffuse scattering in the wide-angle region around 0.51 - 0.57 nm; attributed to the lateral distances of the side-chains confirms the fluid nature of the cholesterol-based liquid crystals (Figures 3 and S15-S17).[36,37] . The shift to smaller

values with decreasing temperature is typical for such systems and is associated with reduced mobility at lowering the temperature and tighter packing. The layer thickness differs somewhat for the various LC-homo and block copolymers with respect to temperature, the layer spacings are at 5.00 ± 0.18 nm. The length of a cholesterol side-chain is about 2.9 nm in all-trans formation. This suggests the formation of a lamellar structure of double layers. This can be achieved by interdigitation of the cholesterol end chains. For homopolymers, the layer spacings increase initially on cooling; attributed to an increase of the average ordering perpendicular to the layer normal with reduced temperature and level out (the insets of Figure 3 and Figures S15 & S16) at low temperatures. For the copolymers, the picture is somewhat more complex. It was found that on cooling from the isotropic the size of the layer spacing increases with decreasing temperature, as observed for the homopolymers, but at specific temperatures, the layer spacings start to decrease on cooling further. For the polymers with long PMMA chains this coincides with the formation of "*schlieren*" textures and thus is associated with the formation of the SmC* phase (the insets of Figure 3 and Figures S15 & S16). For the systems with the short PMMA blocks, such as $PChMA_{24}$-*b*-$PMMA_{27}$, $PChMA_{40}$-*b*-$PMMA_{32}$, $PChMA_{40}$-*b*-$PMMA_{46}$ no such optical transition was observed; the *batonnêt* containing textures remain; hence further investigation of the assembly behaviour was needed. Common for all systems is that no corresponding transition peaks in the DSC traces could be detected, the data suggests that the block copolymers show either a second-order phase transition from the smectic A (SmA*) to the smectic C phase (SmC*); or alternatively, a weak first order transition could be distributed over a wider temperature range when compared to that of low molar mass liquid crystals. This could due to the polydispersity of the sample and the presence of non – LC blocks. The emergence of

tilted cholesterol groups in the smectic C phase reduces the layer thickness of the layers compared to the smectic A phase where the cores are on average perpendicular to the layer normal (Figures 3, S15 and S16). This can be rationalized as a function of the presence of the PMMA blocks which due to their smaller volume reduces the steric hindrance and provide the free volume permitting the tilting of cholesteryl mesogens, and controlling the layer thickness of LC-BCPs. The synclinic arrangement of the SmC phase as shown in Figure 4 is proposed, based on the formation of chiral optical signals in thin films in POM experiments and the simple bilayer structure in the SAXS experiments. We note that the SmC phase is rarely observed in cholesteryl based polymers as the aromatic and dipole groups, typically associated with the formation of a SmC phase in thermotropic polymers are lacking. In the case reported here, this layered phase is a function of space filling requirements, achieved most easily by tilting the mesogenic groups. For the BCPs with the short PMMA blocks this does not seem to occur, a different ordering mechanism takes place.

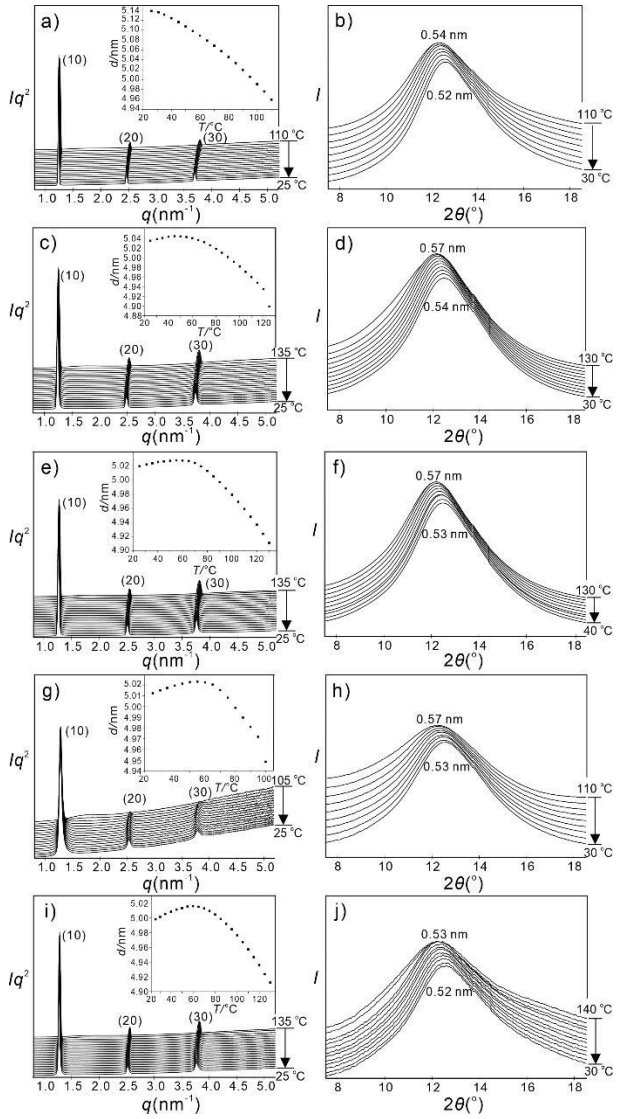

Figure 3. SAXS and WAXS diffractograms of (a, b) SmA* phase of LC-homo ($PChMA_{40}$); SmA* to SmC* phase transition during the 1st cooling process of (c, d) $PChMA_{40}$-*b*-$PMMA_{32}$, (e, f) $PChMA_{40}$-*b*-$PMMA_{46}$, (g, h) $PChMA_{40}$-*b*-$PMMA_{52}$ and (i, j) $PChMA_{40}$-*b*-$PMMA_{78}$). The insets in (a, c, e, g and i) show layer thickness *vs.* temperature.

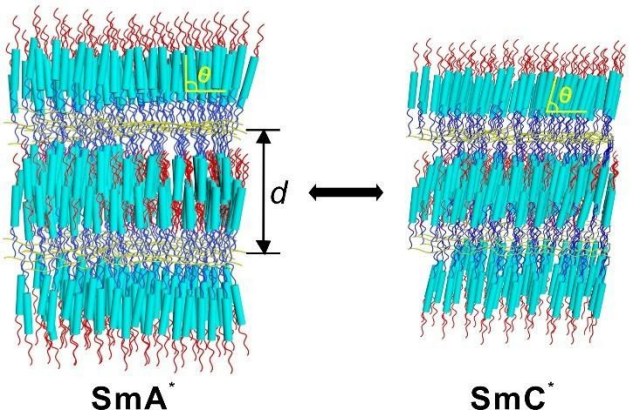

Figure 4. Schematic illustration of the bilayer structure of the intercalated molecules in the rod-like conformation of SmA* and SmC* phases of LC-BCPs. (Sky blue Rod indicates the Cholesterol mesogen; Red line represents the alkyl chains; Yellow line indicates the main chain of the polymer; and blue line represents the hexyl (C6) spacer). (* indicates the presence of chiral mesogens in LC-BCPs).

Circular Dichroism of the cholesterol derived LC-homo and BCPs

To measure and investigate the differences between BCPs with short and long PMMA blocks we performed precise thin-film CD analysis for LC-BCPs. For measurements, all in the SmA phase, polymeric thin films were prepared so that homeotropic orientation was achieved; the molecules are parallel to the beam. The samples were rotated in the plane at 45° intervals to detect and exclude the influence of linear dichroism (LD) and linear birefringence (LB) (Figures S18-S20).[38-40] However, as the thickness of the samples was not strictly uniform and the number of chiral groups varies in this set of materials; *eg.* short and long blocks, the CD results are discussed on the basis of the sign, and not the peak intensity. Overall two modes of behaviour were detected. PChMA homopolymers and BCPs with long PMMA blocks behaved similar, a

positive Cotton effect which does not change sign on changing temperature was detected; for BCPs with short PMMA chains a reversal of the Cotton effect at low temperatures from positive to negative going with descending temperatures was detected; this is associated with an inversion of chirality. In detail, the cholesterol-based homopolymers ($PChMA_{12}$, $PChMA_{24}$, and $PChMA_{40}$) were found to exhibit a positive cotton effect with maxima at 276 nm, 264 nm and 275 nm (Figure S21). The signal intensity increases somewhat with decreasing temperature. This is in line with the closer packing observed by SAXS and the corresponding enhanced chirality synchronization at low temperatures.[41,42]

Surprisingly, in the case of $PChMA_{24}$-*b*-$PMMA_{27}$ positive and negative values for the Cotton effect with peaks at maxima at 256 and 285 nm, respectively, at 30 °C were detected, corresponding to absorption bands of the cholesterol mesogens, which are reversed to the case at 50 °C, where negative and positive values with maxima at 260 and 282 nm were found (Figure 5a). As a further example of $PChMA_{40}$-*b*-$PMMA_{32}$ a positive cotton effect (30 °C) is completely reversed at 40 °C and 50 °C in a wide spectral range (Figure 5b) was measured. Extended the PMMA chain slightly for $PChMA_{40}$-*b*-$PMMA_{46}$ it was found to exhibit a negative, positive and negative cotton effect with peaks at maxima of 253, 277 and 284 nm at 30 °C, which are reversed peaks with maxima at 262, 274 and 291 nm at 50 °C (Figure S22). The reversal of the signal is evidence of a dramatic change of the chirality in the thin film. From the series of the investigated LC-BCPs, three of the BCPs, $PChMA_{24}$-*b*-$PMMA_{27}$, $PChMA_{40}$-*b*-$PMMA_{32}$ and $PChMA_{40}$-*b*-$PMMA_{46}$ displayed the strongest temperature-driven chirality inversion at a specific temperature range, and there no inversion of chirality at high-temperatures was observed (Figures S23-S25). A possible reason for the bisignate CD signals/inversion of chirality is the

presence of methyl substituted blocks in the polymethacrylate linked LC mesogen, sterically impacting on the packing of the polymers with less tilted cholesterol mesogens. The restricted rotation of the PMMA blocks generating a range of conformers in these side-chain polymers.[35] Moreover, the conformational shape of the polymeric backbone is responsible for the orientation of the attached LC mesogen relative to the backbone itself.[19,43,44] As the LC mesogens are separated from the polymer backbone this causes less hindrance and free rotation of the PMMA blocks at moderate range of PMMA blocks is possible. This is in line with the bisignate signal in a wide range of spectral wavelengths and no chirality inversion was observed between 90 °C to 30 °C. In some cases, LC-BCPs with high DP's of PMMA blocks showed only a positive cotton effect (without sign reversal) at a broad range of spectral wavelengths (Figures S23-S25). From these results, we concluded that smaller PMMA blocks with repeats ranging from 27-40 units play a major role in the chirality inversion process of the LC-BCPs. The BCPs with short PMMA blocks containing a large syndiotactic component (53.3 %) have strong steric interaction between the block molecules, and they form conformers with the LC blocks (Figure S26) which change the overall helicity. For long PChMA and PMMA blocks at lower temperatures the data indicates that the cholesteryl groups seem to be able to tilt sufficiently uniformly in a block allowing for SmC* phase formation. For shorter chains the combination of space filling requirements and conformations of the main chain does not allow this; the SmA* phase is retained but the phase chirality is inverted.

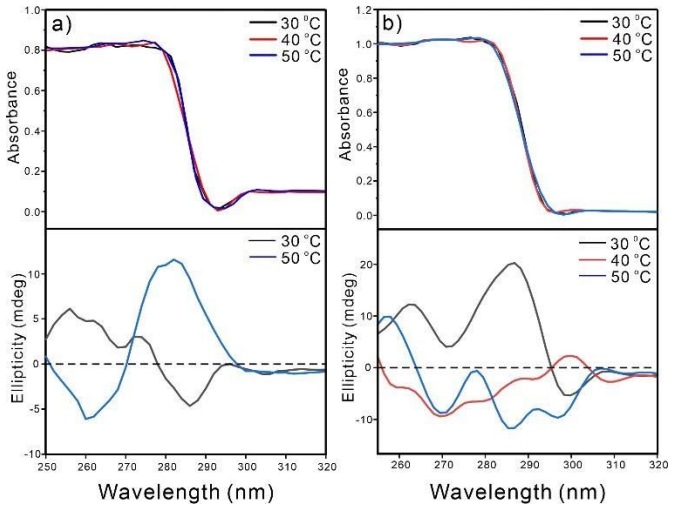

Figure 5. Temperature-dependent CD spectra of thin films of LC-BCPs: a) $PChMA_{24}$-*b*-$PMMA_{27}$, b) $PChMA_{40}$-*b*-$PMMA_{32}$ at various temperatures.

Electronic properties and Conformational analysis

The electronic transition properties of the LC-BCPs were evaluated experimentally and theoretically, in order to understand the nature of electronic transitions present in the polymers. Simulations of the UV-vis and CD spectra were carried out on the TD-DFT/B3LYP/6-31+G(d,p) basis level. The simulated and experimental electronic transition spectra of LC-BCPs are observed at 267 nm and 264 nm, which is closely matched with experimental value as shown in Table S2. For LC-BCPs, the electron density distribution of the highest occupied molecular orbitals (HOMO) over cholesterol moiety, while in contrast the lowest unoccupied molecular orbitals (LUMO) located in the dithiobenzoate region of the LC-BCP, which indicates that the intramolecular charge (ICT) process[45,46] from the electron donor HOMO to electron acceptor (LUMO) group (Figure S27).

The conformational analysis of the LC-BCPs was carried out to identify their ground-state geometry through Density functional theory (DFT) calculation.[47] The potential energy surface (PES) scan was performed as a function of PMMA-thiol linkage dihedral angle (C_2-S_{21}-C_{15}-C_{20}) with a fixed cholesteryl unit by varying the dihedral angles for every 10 degrees of rotation at B3LYP/6-31G(d,p) basis set level. The LC-BCP possesses two equally possible conformers such as *syn*- and *anti*-forms with different energy levels as shown in Figure 6 (Figure S28). From the PES curve, the highest energy domain of *syn*-form is located at 116° (-3309.2861 Hartree) and the lower energy of anti-form is located at 66° (-3309.29106 Hartree). In comparison, the anti-form possesses global minima, which exhibits a more stable conformer than *syn*-form.[48] In addition, the energy barrier between the *syn*- and *anti*-forms is 13 kJ/mol. This significant energy difference would facilitate rapid changes in the various conformation of PMMA blocks present in the LC-BCPs. Simulated CD spectra of LC-BCP with dihedral angles 66° and 116° are opposite (Figure 6b). This reveals that the observed CD sign of LC-BCPs reflects the global minima of PMMA-thiol linkage induced by different conformers of PMMA blocks.

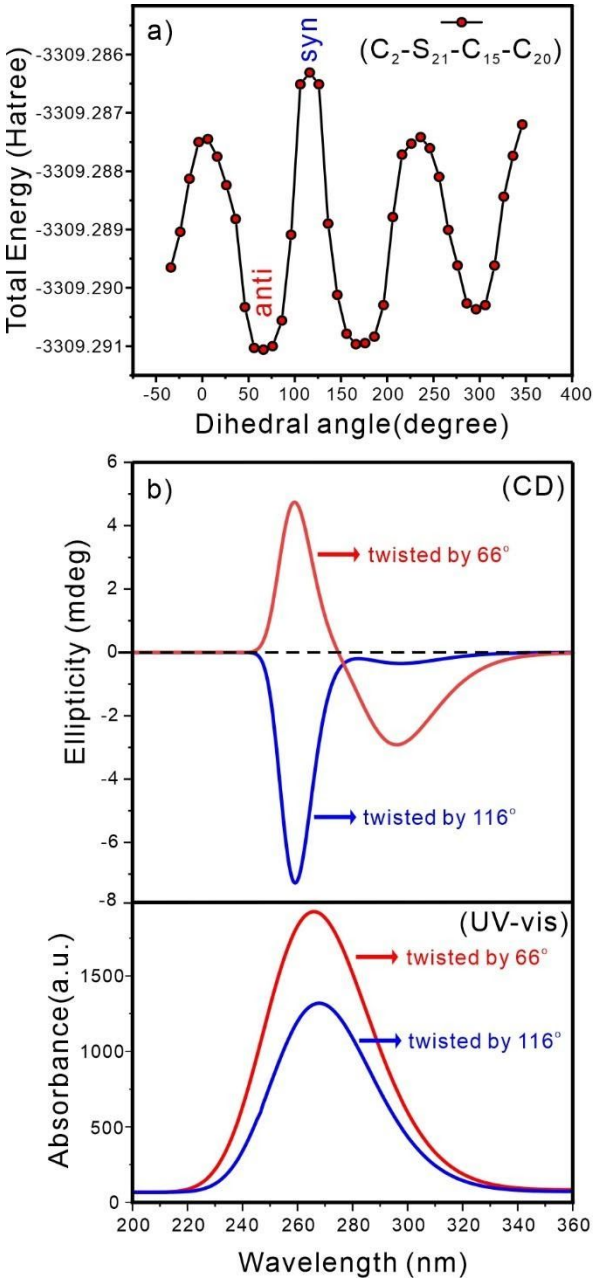

Figure 6. DFT simulation: (a) potential energy surface of LC-BCP as a function of PMMA-thiol dihedral angle (C_2-S_{21}-C_{15}-C_{20}) with fixed cholesterol moiety; (b) simulated UV-*vis* and CD spectra of LC-BCP (PMMA-thiol dihedral angle 66° and 116°).

CONCLUSIONS

In summary, we explored the mesophase mediated self-assembly structures of well-defined block copolymers with a methacrylate main chain. The block size was systematically varied; consisting of two incompatible blocks; one a cholesteryl unit as a rigid block and the other a methyl group as a soft block. The polymers were prepared by RAFT polymerization and the block sizes of the block copolymers were varied systematically in size and measured by GPC and the regiochemistry of the backbone was identified by detailed NMR studies identifying pentads of the repeat units. Mesophase formation is controlled by the size of the polymers and the block composition. For block copolymers (PChMA-*b*-PMMA) consisting of large PMMA blocks the phase sequence SmA*- SmC* was detected, based on DSC, POM, and synchrotron SAXS studies; while for polymers containing short PMMA blocks, no SmC* phase was formed, instead chirality inversion occurs as measured by temperature dependent CD spectroscopy in thin films and supported by DFT simulations. Notable is the absence of signals for superstructures based on microsegregation of chemically different blocks, a typical means for block co-polymers to minimize energy.

We identify the chirality inversion in the short block polymers as the predominantly syndiotactic tacticity of the PChMA blocks, which prevent efficient packing for those with low ratio of PMMA block at low temperatures – such as the formation of SmC* structures of the cholesteryl units. The polymers escape the energy penalty at low temperatures by finding low energy conformations associated with a chirality inversion in the CD signals associated with the cholesteryl groups; whilst SAXS and POM data indicate that an overall lamellar ordering is

maintained. The effect measured here may be present at some of the temperature-driven helix-helix transitions in nature and has the potential to be exploited further for artificial systems.

ASSOCIATED CONTENT

Supporting Information

Experimental methods, NMR, DSC, POM, SAXS, WAXS, CD and theoretical calculation results are included in the supporting information.

AUTHOR INFORMATION

Corresponding Author

*E-mail: feng.liu@xjtu.edu.cn.

*E-mail: qilu.zhang@xjtu.edu.cn.

*E-mail: g.h.mehl@hull.ac.uk.

Notes

The authors declare no competing financial interest.

ACKNOWLEDGMENTS

This work is supported by National Natural Science Foundation of China (No. 21774099 and 51603166) and Science and Technology Agency of Shaanxi Province (2016KW-050, 2018KW-008 and 2018KWZ-03). The authors also thank for financial support by 111 Project 2.0 (BP2018008). Part of the characterization was performed at Instrument Analysis Center of Xi'an Jiaotong University. For help with synchrotron experiments, the authors thank the staff at beamlines BL16B1 at Shanghai Synchrotron Radiation Facility.

REFERENCES

(1) Kato, T. Self-assembly of phase-segregated liquid crystal structures. *Science* **2002**, *295*, 2414-2418.

(2) Lazzari, M.; Lopez-Quintela, M. A. Block copolymers as a tool for nanomaterial fabrication. *Adv. Mater.* **2003**, *15*, 1583-1594.

(3) Cheng, X. H.; Ju, X. P.; Ye, H. Synthesis and mesophase characterization of block molecules with different topologies. *Prog. Chem.* **2006**, *18*, 1626-1633.

(4) Bates, C. M.; Maher, M. J.; Janes, D. W.; Ellison, C. J.; Willson, C. G. Block Copolymer Lithography. *Macromolecules* **2014**, *47*, 2-12.

(5) Tschierske, C. Development of Structural Complexity by Liquid-Crystal Self-assembly. *Angew. Chem. Int. Edit.* **2013**, *52*, 8828-8878.

(6) Jiang, X. Q.; Zhao, R. Y.; Chang, W. Y.; Yin, D. X.; Guo, Y. C.; Wang, W.; Liang, D. H.; Yang, S.; Shi, A. C.; Chen, E. Q. Highly Ordered Sub-10 nm Patterns Based on Multichain Columns of Side-Chain Liquid Crystalline Polymers. *Macromolecules* **2019**, *52*, 5033-5041.

(7) Liao, F.; Shi, L. Y.; Cheng, L. C.; Lee, S.; Ran, R.; Yager, K. G.; Ross, C. A. Self-assembly of a silicon- containing side- chain liquid crystalline block copolymer in bulk and in thin films: kinetic pathway of a cylinder to sphere transition. *Nanoscale* **2019**, *11*, 285-293.

(8) Jin, B. X.; Sano, K.; Aya, S.; Ishida, Y.; Gianneschi, N.; Luo, Y. J.; Li, X. Y. One-pot universal initiation-growth methods from a liquid crystalline block copolymer. *Nat. Commun.* **2019**, *10*, 2397.

(9) Chen, X. F.; Shen, Z. H.; Wan, X. H.; Fan, X. H.; Chen, E. Q.; Ma, Y. G.; Zhou, Q. F. Mesogen-jacketed liquid crystalline polymers. *Chem. Soc. Rev.* **2010**, *39*, 3072-3101.

(10) Mai, Y. Y.; Eisenberg, A. Self-assembly of block copolymers. *Chem. Soc. Rev.* **2012**, *41*, 5969-5985.

(11) Ke, X. X.; Wang, L.; Xu, J. T.; Du, B. Y.; Tu, Y. F.; Fan, Z. Q. Effect of local chain deformability on the temperature-induced morphological transitions of polystyrene-*b*-poly(N-isopropylacrylamide) micelles in aqueous solution. *Soft Matter* **2014**, *10*, 5201-5211.

(12) Wen, W.; Huang, T. Y.; Guan, S.; Zhao, Y. B.; Chen, A. H. Self-Assembly of Single Chain Janus Nanoparticles with Tunable Liquid Crystalline Properties from Stilbene-Containing Block Copolymers. *Macromolecules* **2019**, *52*, 2956-2964.

(13) Jenekhe, S. A.; Chen, X. L. Self-assembled aggregates of rod-coil block copolymers and their solubilization and encapsulation of fullerenes. *Science* **1998**, *279*, 1903-1907.

(14) Shi, L. Y.; Lee, S.; Cheng, L. C.; Huang, H. J.; Liao, F.; Ran, R.; Yager, K. G.; Ross, C. A. Thin Film Self-Assembly of a Silicon-Containing Rod-Coil Liquid Crystalline Block Copolymer. *Macromolecules* **2019**, *52*, 679-689.

(15) Jia, L.; Albouy, P. A.; Di Cicco, A.; Cao, A.; Li, M. H. Self-assembly of amphiphilic liquid crystal block copolymers containing a cholesteryl mesogen: Effects of block ratio and solvent. *Polymer* **2011**, *52*, 2565-2575.

(16) Zhang, L. Y.; Yao, W. H.; Gao, Y. Z.; Zhang, C. H.; Yang, H. Polysiloxane-Based Side Chain Liquid Crystal Polymers: From Synthesis to Structure-Phase Transition Behavior Relationships. *Polymers* **2018**, *10*, 794.

(17) Smulders, M. M. J.; Filot, I. A. W.; Leenders, J. M. A.; van der Schoot, P.; Palmans, A. R. A.; Schenning, A. P. H. J.; Meijer, E. W. Tuning the Extent of Chiral Amplification by Temperature in a Dynamic Supramolecular Polymer. *J. Am. Chem. Soc.* **2010**, *132*, 611-619.

(18) Sun, R. Y.; Xue, C. M.; Ma, X.; Gao, M.; Tian, H.; Li, Q. Light-Driven Linear Helical Supramolecular Polymer Formed by Molecular-Recognition-Directed Self-Assembly of Bis(p-sulfonatocalix[4]arene) and Pseudorotaxane. *J. Am. Chem. Soc.* **2013**, *135*, 5990-5993.

(19) Nishiyama, I.; Goodby, J. W. Effect of Polymerization on the Stability of Antiferroelectric Liquid-Crystalline Phases - Liquid-Crystalline Properties of Some Chiral Acrylates and Their Corresponding Polyacrylates. *J. Mater. Chem.* **1993**, *3*, 169-182.

(20) Cao, H.; Zhu, X. F.; Liu, M. H. Self-Assembly of Racemic Alanine Derivatives: Unexpected Chiral Twist and Enhanced Capacity for the Discrimination of Chiral Species. *Angew. Chem. Int. Edit.* **2013**, *52*, 4122-4126.

(21) Inoue, Y.; Matsushima, E.; Wada, T. Pressure and temperature control of product chirality in asymmetric photochemistry. Enantiodifferentiating photoisomerization of cyclooctene sensitized by chiral benzenepolycarboxylates. *J. Am. Chem. Soc.* **1998**, *120*, 10687-10696.

(22) Yao, J. B.; Wu, W. H.; Liang, W. T.; Feng, Y. J.; Zhou, D. Y.; Chruma, J. J.; Fukuhara, G.; Mori, T.; Inoue, Y.; Yang, C. Temperature-Driven Planar Chirality Switching of a Pillar[5]arene-Based Molecular Universal Joint. *Angew. Chem. Int. Edit.* **2017**, *56*, 6869-6873.

(23) Fujiki, M.; Koe, J. R.; Motonaga, M.; Nakashima, H.; Terao, K.; Teramoto, A. Computing handedness: Quantized and superposed switch and dynamic memory of helical polysilylene. *J. Am. Chem. Soc.* **2001**, *123*, 6253-6261.

(24) Fujiki, M. Helix magic. Thermo-driven chiroptical switching and screw-sense inversion of flexible rod helical polysilylenes. *J. Am. Chem. Soc.* **2000**, *122*, 3336-3343.

(25) Tang, K.; Green, M. M.; Cheon, K. S.; Selinger, J. V.; Garetz, B. A. Chiral conflict. The effect of temperature on the helical sense of a polymer controlled by the competition between structurally different enantiomers: From dilute solution to the lyotropic liquid crystal state. *J. Am. Chem. Soc.* **2003**, *125*, 7313-7323.

(26) Zhou, Y. X.; Ahn, S. K.; Lakhman, R. K.; Gopinadhan, M.; Osuji, C. O.; Kasi, R. M. Tailoring Crystallization Behavior of PEO-Based Liquid Crystalline Block Copolymers through Variation in Liquid Crystalline Content. *Macromolecules* **2011**, *44*, 3924-3934.

(27) Chiefari, J.; Chong, Y. K.; Ercole, F.; Krstina, J.; Jeffery, J.; Le, T. P. T.; Mayadunne, R. T. A.; Meijs, G. F.; Moad, C. L.; Moad, G.; Rizzardo, E.; Thang, S. H. Living free-radical polymerization by reversible addition-fragmentation chain transfer: The RAFT process. *Macromolecules* **1998**, *31*, 5559-5562.

(28) Moad, G.; Rizzardo, E.; Thang, S. H. Living Radical Polymerization by the RAFT Process - A Third Update. *Aust. J. Chem.* **2012**, *65*, 985-1076.

(29) Gaborieau, M.; Castignolles, P. Size-exclusion chromatography (SEC) of branched polymers and polysaccharides. *Anal. Bioanal. Chem.* **2011**, *399*, 1413-1423.

(30) Brar, A. S.; Singh, G.; Shankar, R. Structural investigations of poly(methyl methacrylate) by two-dimensional NMR. *J. Mol. Struct.* **2004**, *703*, 69-81.

(31) Matlengiewicz, M.; Nguyen, G.; Nicole, D.; Henzel, N. Analysis of β-CH_2 signals in the ^{13}C NMR spectra of the methyl methacrylate-ethyl acrylate copolymer as a tool for microstructure determination. *J. Polym. Sci. Pol. Chem.* **2000**, *38*, 2147-2155.

(32) Kawamura, T.; Toshima, N.; Matsuzaki, K. Assignment of Finely Resolved ^{13}C Nmr-Spectra of Poly(Methyl Methacrylate). *Makromol. Chem.-Rapid.* **1993**, *14*, 719-724.

(33) Champagne, P. L.; Ester, D.; Polan, D.; Williams, V. E.; Thangadurai, V.; Ling, C. C. Amphiphilic Cyclodextrin-Based Liquid Crystals for Proton Conduction. *J. Am. Chem. Soc.* **2019**, *141*, 9217-9224.

(34) Chain, S. H.; Rodriguezparada, J. M.; Percec, V. Liquid-Crystalline Polymers Containing Heterocycloalkanediyl Groups as Mesogens .1. Liquid-Crystalline Polymethacrylates and Polyacrylates Containing 1,3-Dioxane-2,5-Diyl Groups as Mesogens in the Side-Chain. *Makromol. Chem*. **1987**, *188*, 1017-1031.

(35) Bolton, E. C.; Lacey, D.; Smith, P. J.; Goodby, J. W. Twisted Smectic-a Phases in Side-Chain Liquid-Crystal Polymers. *Liq. Cryst.* **1992**, *12*, 305-318.

(36) Chan, T.-N.; Yeap, G.-Y.; Yam, W.-S.; Madrak, K.; Zep, A.; Pociecha, D.; Gorecka, E. A crossover from rod-shaped to bent-shaped in symmetric isoflavone liquid crystal trimers exhibiting unusual mesomorphic behaviour. *J. Mater. Chem.* **2012**, *22*, 11335-11339.

(37) Tan, X. P.; Zhang, R. L.; Guo, C. X.; Cheng, X. H.; Gao, H. F.; Liu, F.; Bruckner, J. R.; Giesselmann, F.; Prehm, M.; Tschierske, C. Amphotropic azobenzene derivatives with oligooxyethylene and glycerol based polar groups. *J. Mater. Chem. C* **2015**, *3*, 11202-11211.

(38) Saeva, F. D.; Olin, G. R. Extrinsic Circular-Dichroism in Twisted Nematic Mesophases. *J. Am. Chem. Soc.* **1976**, *98*, 2709-2711.

(39) Sharma, A.; Mori, T.; Lee, H. C.; Worden, M.; Bidwell, E.; Hegmann, T. Detecting, Visualizing, and Measuring Gold Nanoparticle Chirality Using Helical Pitch Measurements in Nematic Liquid Crystal Phases. *Acs Nano* **2014**, *8*, 11966-11976.

(40) Cseh, L.; Mang, X. B.; Zeng, X. B.; Liu, F.; Mehl, G. H.; Ungar, G.; Siligardil, G. Helically Twisted Chiral Arrays of Gold Nanoparticles Coated with a Cholesterol Mesogen. *J. Am. Chem. Soc.* **2015**, *137*, 12736-12739.

(41) Soininen, A. J.; Kasemi, E.; Schluter, A. D.; Ikkala, O.; Ruokolainen, J.; Mezzenga, R. Self-Assembly and Induced Circular Dichroism in Dendritic Supramolecules with Cholesteric Pendant Groups. *J. Am. Chem. Soc.* **2010**, *132*, 10882-10890.

(42) Ye, Q.; Zhu, D. D.; Zhang, H. X.; Lu, X. M.; Lu, Q. H. Thermally tunable circular dichroism and circularly polarized luminescence of tetraphenylethene with two cholesterol pendants. *J. Mater. Chem. C* **2015**, *3*, 6997-7003.

(43) Fujiki, M.; Toyoda, S.; Yuan, C. H.; Takigawa, H. Near-UV, circular dichroism, and fluorescence spectra of a rigid rodlike helical polysilane bearing trietheral moiety in ethanol/water. *Chirality* **1998**, *10*, 667-675.

(44) Wang, L. B.; Yin, L.; Zhang, W.; Zhu, X. L.; Fujiki, M. Circularly Polarized Light with Sense and Wavelengths To Regulate Azobenzene Supramolecular Chirality in Optofluidic Medium. *J. Am. Chem. Soc.* **2017**, *139*, 13218-13226.

(45) Sridevi, C.; Shanthi, G.; Velraj, G. Structural, vibrational, electronic, NMR and reactivity analyses of 2-amino-4H-chromene-3-carbonitrile (ACC) by ab initio HF and DFT calculations. *Spectrochim. Acta A* **2012**, *89*, 46-54.

(46) Sridevi, C.; Velraj, G. Structural, vibrational, electronic, NMR, NLO and reactivity analyses of (3Z)-3-(2-oxo-2-phenylethylidene)-1,3-dihydro-2H-indol-2-one (OPEDI) by ab initio HF and DFT calculations. *Spectrochim. Acta A* **2013**, *107*, 334-346.

(47) Frisch, M. J.; Trucks, G. W.; Schlegel, H. B.; Scuseria, G. E.; Robb, M. A.; Cheeseman, J. R.; Scalmani, G.; Barone, V.; Petersson, G. A.; Nakatsuji, H.; Li, X.; Caricato, M.; Marenich, A.; Bloino, J.; Janesko, B. G.; Gomperts, R.; Mennucci, B.; Hratchian, H. P.; Ortiz, J. V.; Izmaylov, A. F.; Sonnenberg, J. L.; Williams-Young, D.; Ding, F.; Lipparini, F.; Egidi, F.; Goings, J.; Peng, B.; Petrone, A.; Henderson, T.; Ranasinghe, D.; Zakrzewski, V. G.; Gao, J.; Rega, N.; Zheng, G.; Liang, W.; Hada, M.; Ehara, M.; Toyota, K.; Fukuda, R.; Hasegawa, J.; Ishida, M.; Nakajima, T.; Honda, Y.; Kitao, O.; Nakai, H.; Vreven, T.; Throssell, K.; Montgomery, Jr. J. A.; Peralta, J. E.; Ogliaro, F.; Bearpark, M.; Heyd, J. J.; Brothers, E.; Kudin, K. N.; Staroverov, V. N.; Keith, T.; Kobayashi, R.; Normand, J.; Raghavachari, K.; Rendell, A.; Burant, J. C.; Iyengar, S. S.; Tomasi, J.; Cossi, M.; Millam, J. M.; Klene, M.; Adamo, C.; Cammi, R.; Ochterski, J. W.; Martin, R. L.; Morokuma, K.; Farkas, O.; Foresman, J. B.; Fox, D. J. Gaussian, Inc., Wallingford CT, **2009**.

(48) James, C.; Pettit, G. R.; Nielsen, O. F.; Jayakumar, V. S.; Joe, I. H. Vibrational spectra and ab initio molecular orbital calculations of the novel anti-cancer drug combretastatin A-4 prodrug. *Spectrochim. Acta A* **2008**, *70*, 1208-1216.

(49) Ferji K.; Nouvel C.; Babin J.; Albouy P.-A.; Li M.-H.; Six J.-L. Controlled synthesis of new amphiphilic glycopolymers with liquid crystal grafts. *J. Polym. Sci., Part A: Polym. Chem.* **2013**, 51, 3829-3839.

TOC graphical